HadGEM3-GC3.1: The physical coupled model core of UKESM1 now frozen

Till Kuhlbrodt and Colin Jones, *NCAS and UKESM core group*
Ed Blockley and Helene Hewitt*, Met Office Hadley Centre*
Alistair Sellar*, Met Office Hadley Centre and UKESM core group*

UKESM1 is built on top of the core physical model, HadGEM3-GC3.1 (hereafter GC3.1). GC3.1 has primarily been developed for a target atmospheric model resolution of ~60km (N216) and ocean resolution of 0.25° (hereafter N216O025). In addition to this effort, a lower resolution version of GC3.1 has also been developed as the physical model core of UKESM1. The reduced resolution is necessary in order to make UKESM1, with its additional Earth system components, feasible to run for centennial timescale experiments such as planned in the CMIP6 project. This lower resolution version of GC3.1 employs an atmospheric resolution of ~140km (N96) and ocean resolution of 1° (hereafter N96O1). Both models employ the same number of vertical levels, in the atmosphere (85) and ocean (75). Here we present a few key performance metrics for N96O1 and motivate the one difference between the 2 model versions. A detailed analysis of both N216O025 and N96O1 will appear soon in the peer-reviewed literature.

Traceability of parameterizations and parameter settings between model versions

Beyond the standard and necessary differences linked to model resolution (e.g. time step length, viscosity and isopycnal diffusion coefficients and use of a parameterization for mesoscale eddies in the 1° ocean model) a key aim in developing N96O1 was that commonality of model parameterizations and parameter settings with N216O025 was maintained. This was achieved for all parameters except one. To achieve an acceptable simulation of Arctic sea ice thickness it proved necessary to reduce the albedo of snow on sea-ice by 2% in N96O1 for both infra-red (0.70 reduced to 0.68) and visible (0.98 to 0.96) parts of the solar spectrum, with all values well within observational constraints. This change was required due to the 1° ocean model failing to advect sufficient warm water into the Arctic Ocean through the narrow straits connecting the Atlantic with the Arctic (e.g. Denmark and Fram Straits). A consequence of this is sub-surface ocean temperatures are systematically colder (by up to 2°C) in N96O1 than N216O025, leading to sea-ice being up to 1 metre too thick at the end of the Arctic winter in N96O1. Figure 1 illustrates the problem of penetration of water through the Fram Strait in N96O1 compared to N216O025.

In N216O025 two well defined currents are visible across the Fram Strait, with northward directed warm, saline Atlantic water in the eastern half of the strait (right side of figure 1) and southward advection of cold, fresher water in the western portion of the strait. In N96O1, while both currents are visible, they are considerably weaker and more diffuse. This is particularly true for the northward directed warm current, with water on the eastern side of the strait ~2°C colder than in N216O025 and much weaker northward velocities. Similar problems are also seen in the Denmark Strait and appear to be a fundamental problem of the low resolution model poorly resolving these straits. Tests modifying the bathymetry of the Fram and Denmark Straits had little impact on the current structure in either region.

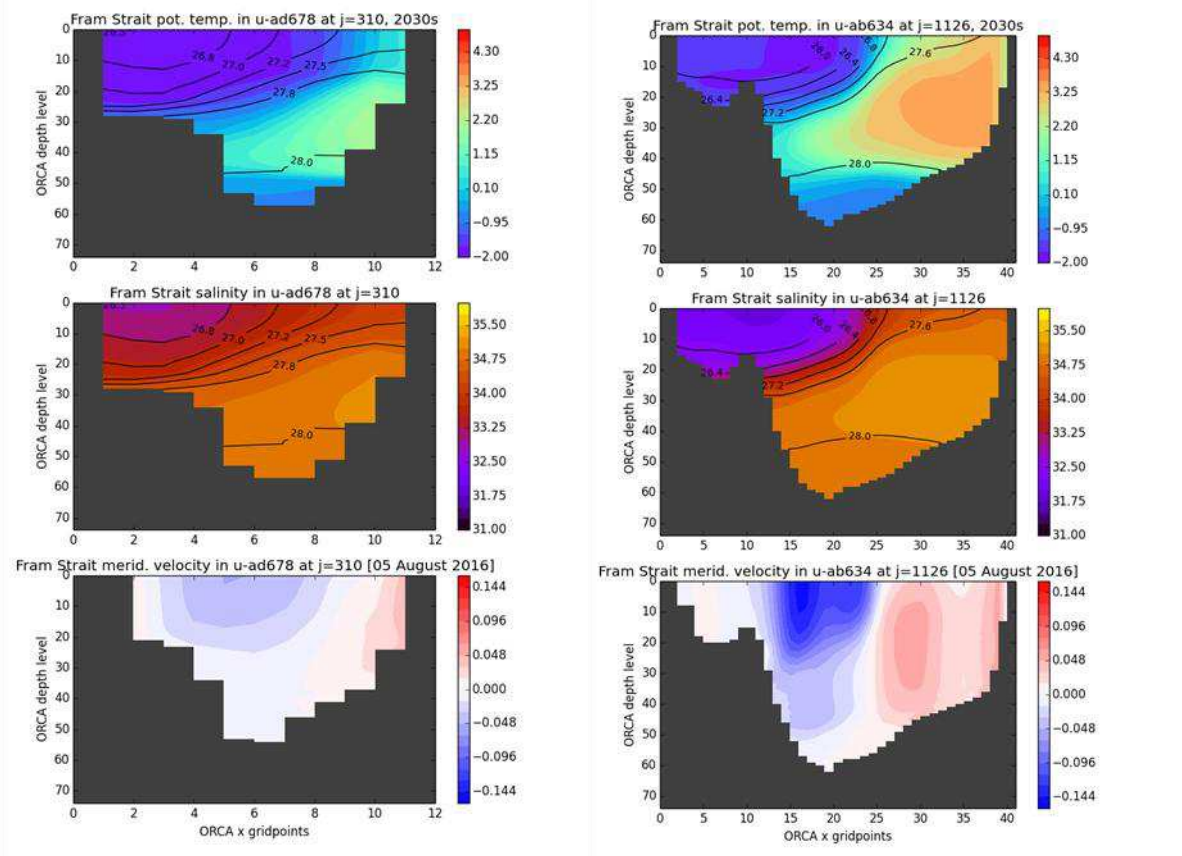

Figure 1. Vertical cross-sections through the Fram Strait of temperature (top), salinity (middle) and northward velocity (bottom): N96O1 (left) and N216O025 (right). Black contours on the upper two rows show ocean potential density.

Weaker penetration of Atlantic water through Fram Strait leads to a cold bias in sub-surface Arctic ocean temperatures and excess sea-ice thickness results from an imbalance between subsurface ice growth and ice melt. A positive bias in sea-ice thickness in the N96O1 simulated present climate will likely cause an incorrect sea-ice response in a future climate. It was therefore decided to remedy this problem through reducing the albedo of snow on sea-ice, compared to that used in N216O025, by 2% in both the infrared and visible solar bands. This results in increased surface melt in N96O1 through solar absorption, balancing the sub-surface bias in growth/melt and results in an accurate simulation of both Arctic sea-ice extent and thickness. Figure 2 (right panel) shows the mean March Arctic sea-ice thickness in N96O1 (top right, experiment af872) and in the same model with the original (2%) higher snow albedo (bottom right, af896). Also shown is the difference in March ice thickness between the 2 experiments, with reduction in ice thickness of up to 1 metre over large parts of the Arctic. Ice thickness in N96O1 is generally closer to observed estimates.

The left panel in Figure 2 plots the mean annual cycle of sea ice extent for both the Arctic (top) and Antarctic (bottom) against the observed sea-ice extent from the HadISST data set (Rayner et al. 2003). In both hemispheres N96O1 ice extent lies within +/-20% of observations throughout the annual cycle. Modification of the snow albedo has only minimal impact on sea ice extent in both hemispheres (compare the red and black annual cycle curves). Furthermore, in the Antarctic the snow albedo reduction also has minimal impact on sea ice thickness (not shown) due to the small

amounts of snow falling onto sea ice in this region. In both hemispheres the timing of maximum ice extent appears to be ~1 month later in the model than in observations. The modification to *snow on sea-ice albedo* is the only parameter difference between the 2 model configurations and is a direct result of the low resolution ocean model poorly resolving key ocean straits and the associated water and heat transport through these straits into the Arctic Ocean.

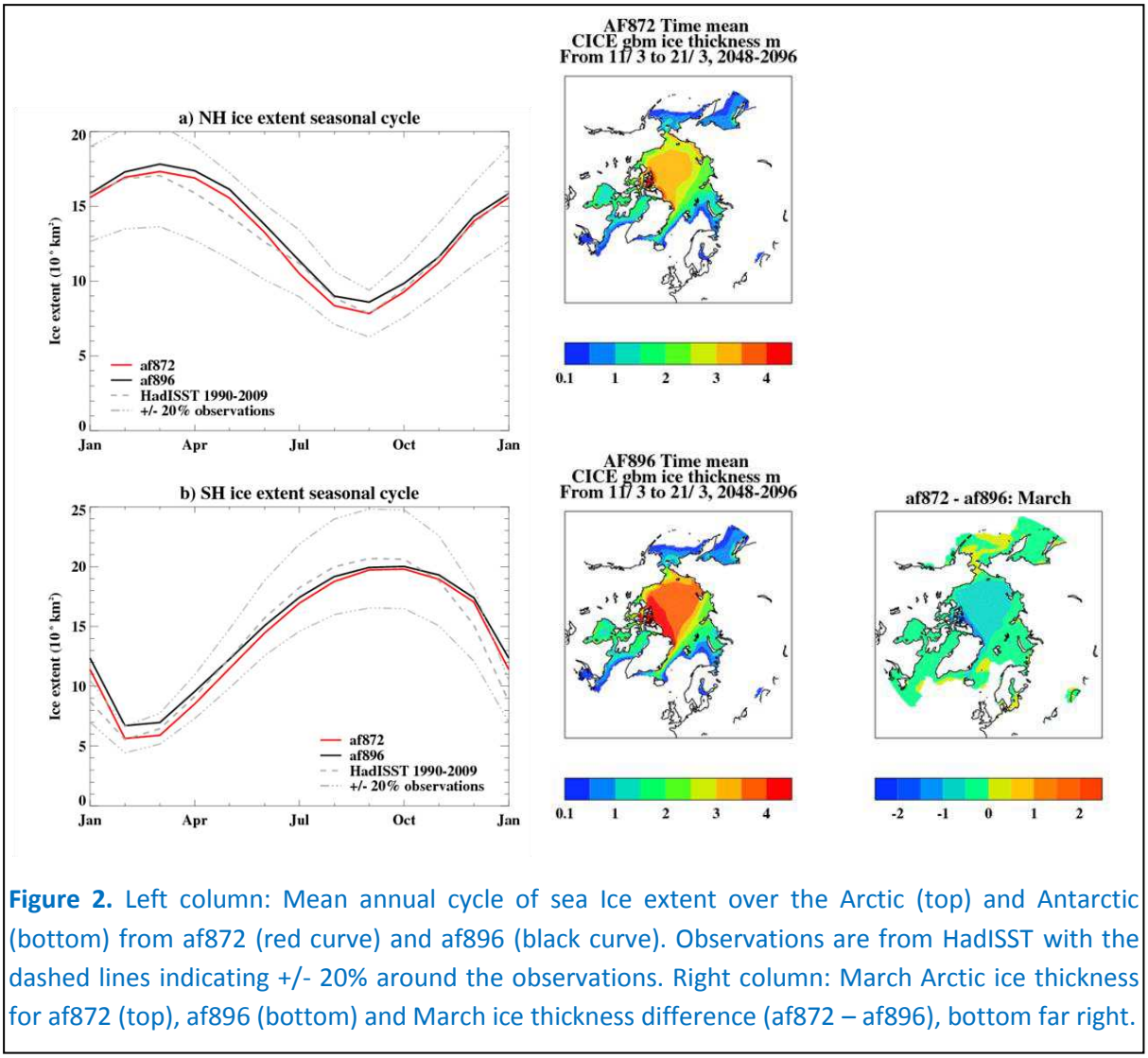

Figure 2. Left column: Mean annual cycle of sea Ice extent over the Arctic (top) and Antarctic (bottom) from af872 (red curve) and af896 (black curve). Observations are from HadISST with the dashed lines indicating +/- 20% around the observations. Right column: March Arctic ice thickness for af872 (top), af896 (bottom) and March ice thickness difference (af872 – af896), bottom far right.

Climatological performance of GC3.1-N96O1

In this section we present a few key performance indicators for N96O1, emphasizing important oceanic parameters. Figure 3 shows biases in model sea surface temperatures (SST) averaged over years 1-20 into a coupled simulation started from EN4 ocean observations (Good et al. 2013) using constant year 2000 forcing (hereafter referred to as PD run). The top left panel shows observed annual mean SSTs for the period 1991-2000. Bottom left shows the bias in annual mean SST in N96O1 relative to these observations and bottom right the same bias for N216O025. The top right panel shows the SST difference (N216O025 minus N96O1) between the 2 model versions. Both models exhibit the same general bias patterns, with a warm bias across the Southern Ocean and an extensive cold bias north of this region (the latter of ~1-2°C). In N96O1 the warm bias over the Southern Ocean is less than in N216O025, by ~1-2°C. In the Northern Hemisphere, SSTs in N96O1 are

also ~1°C colder than N216O025, resulting in the cold SST biases being somewhat worse in this region in N96O1. In the North-East Atlantic a significant cold bias is seen in N96O1 linked to a poor representation of the path of the Gulf Stream and North Atlantic Current across the ocean, a problem common to many low resolution ocean models (Bryan et al. 2007), This is clearly improved in N216O025. Similar problems (albeit of smaller magnitude) are also evident in N96O1 in the North East Pacific, linked to the Kuroshio current, and in the South Atlantic associated with the Brazil current. In all 3 regions N96O1 exhibits systematically colder SSTs than N216O025.

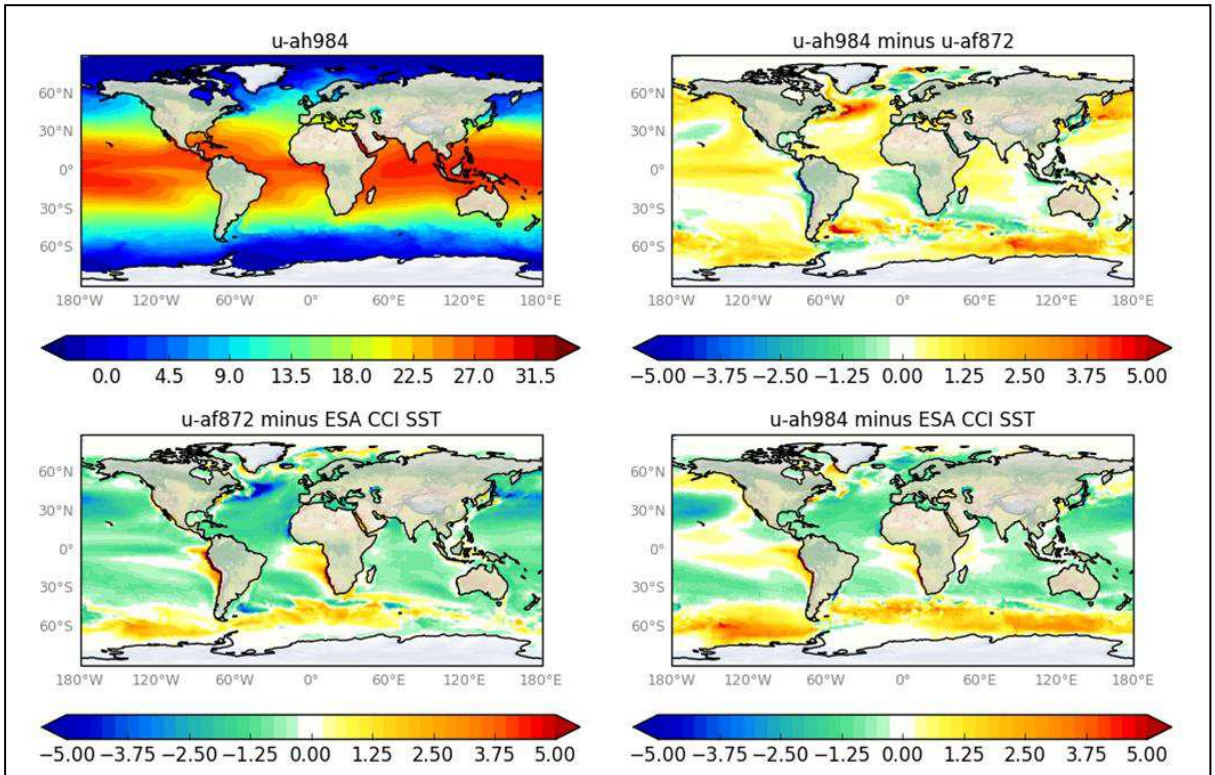

Figure 3. Top left: Observed annual mean SST from the ESA CCI product for 1991-2010, Top Right SST difference: N216O025 minus N96O1. Bottom row shows the bias in the annual mean SST simulated by N96O1 (left) and N216O025 (right).

Figure 4 shows the same annual mean SST bias in N96O1, but now compares the time evolution of these biases through the first 200 years of the PD run. The lower left panel again shows year 1-20 mean SST biases, while the bottom right shows the same SST bias but averaged over years 190-210 into the PD simulation. Top right shows the SST difference in N96O1 between (mean of years 180 to 200) minus (mean of years 1 to 20). The general SST bias patterns remain similar after 200 simulation years, although there is a general tendency for SSTs to warm by ~0.5°C, particularly in the North Atlantic and Pacific.

In figure 5 we plot the annual average global mean SST for the first 185 years of the N96O1 PD simulation. Over the first ~25 years global mean SST cools by ~0.5°C and then gradually warms back towards the observed initial value of ~18.2°C by year 180 of the run. Over this period the vertically averaged global mean ocean temperature (STVAVE) simulated by N96O1 warms at a rate of approximately 0.14°C/year, reflecting that the model is forced by constant year 2000 forcing, with a

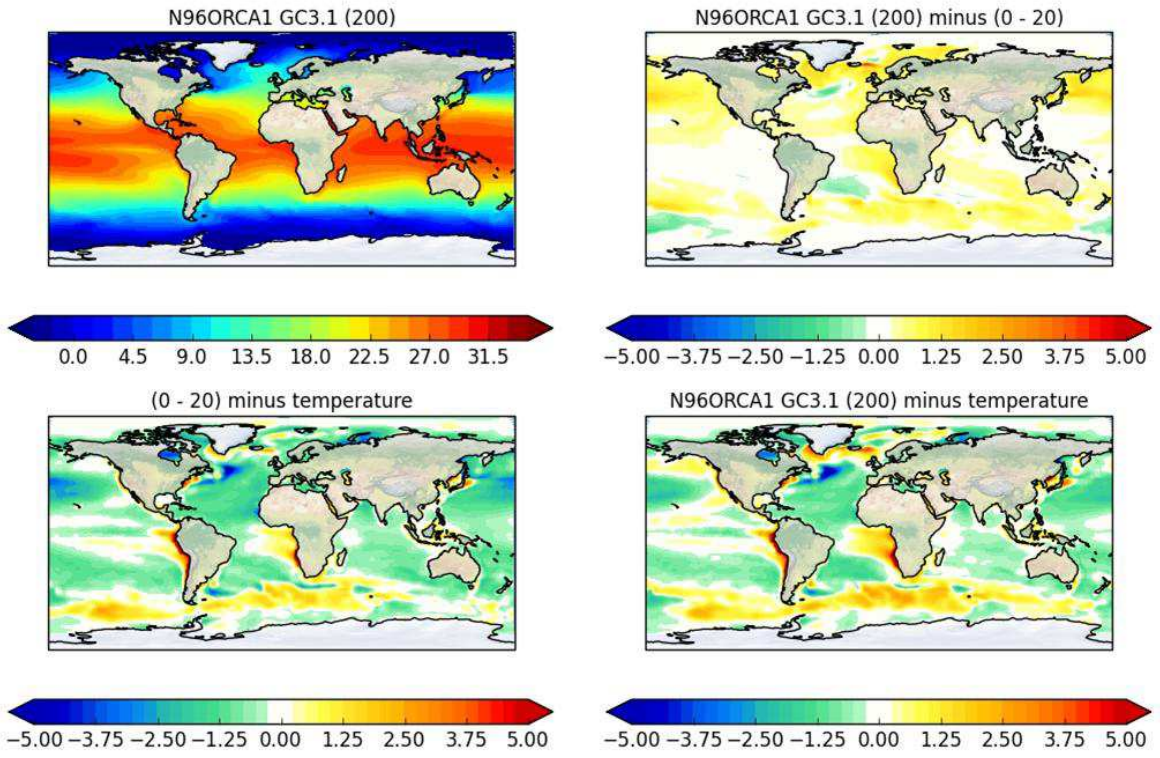

Figure 4. Top left: Observed annual mean SST from the ESA CCI product for 1991-2010, Top Right SST difference year 190-210 minus year 1-20 in N96O1. Bottom row shows the bias in the annual mean SST simulated by N96O1 year 1-20 (left) and years 190-210 (right).

top of atmosphere global mean radiation imbalance of ~+0.5Wm^{-2} (net downward directed energy), while the deep ocean in the EN4 observations is more consistent with pre-industrial forcing. A parallel N96O1 simulation using constant 1850 forcing confirms this with the rate of increase in STVAVE being significantly lower than the year 2000 run, due to the net TOA radiation balance being closer to 0 Wm^{-2}.

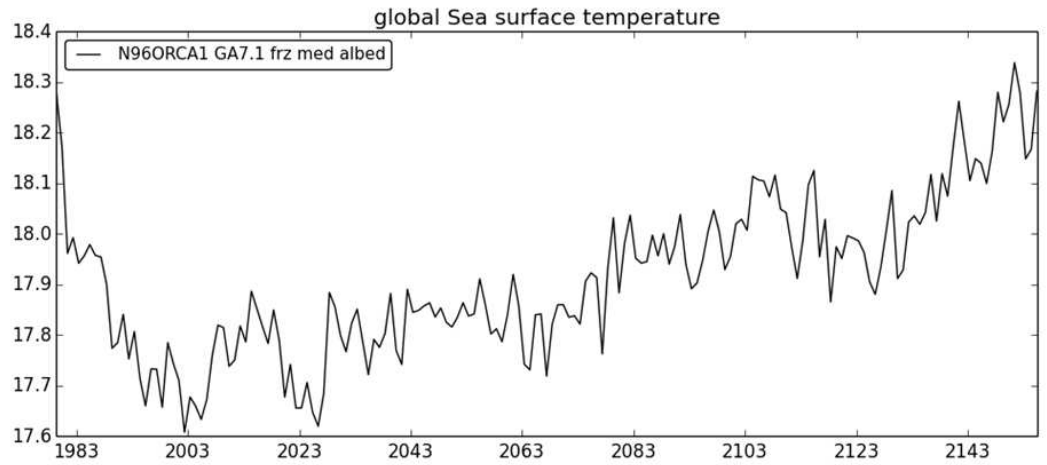

Figure 5. Annually averaged, global mean SST simulated by N96O1 PD simulation.

Finally, in figures 6 and 7 we illustrate the temporal evolution of 2 major features of the global ocean circulation; (i) the Atlantic Meridional Overturning Circulation (AMOC), which plays a key role in transporting heat poleward in the North Atlantic and is a major control on climate variability in both the North Atlantic and Arctic regions (Buckley and Marshall 2016) and (ii) the Antarctic Circumpolar Current (ACC) which transits the entire globe around the Southern Ocean, coincident with a band of atmospheric westerly winds, and plays a key role in the global oceanic overturning circulation (Marshall and Speer 2012), in particular being the main region on Earth where deep ocean water upwells to the surface.

The AMOC in N96O1 initially drops to a value of ~13-14Sv over the first 25 years of the simulation before gradually strengthening over the subsequent 50 years to equilibrate around a mean volume transport (at 26°N) of ~17Sv and multi-annual variability around the mean of ~5Sv. Observations from the RAPID array (Frajka-Williams et al. 2016) indicate a mean meridional volume transport also of ~17Sv, with somewhat larger variability (~8-9Sv) than simulated in N96O1.

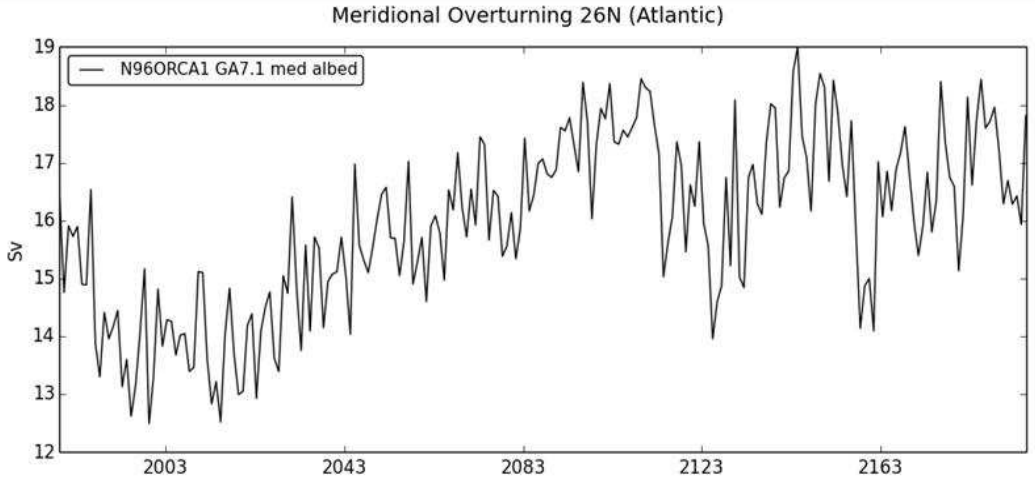

Figure 6. Annual mean meridional transport at 26°N in the Atlantic. Units are Sverdrups (Sv).

Figure 7 shows that the ACC volume transport through the Drake Passage drops from an initial value of 165Sv to 140Sv by year 80 of the PD simulation before stabilizing at a value of ~130-140Sv. This is consistent with the canonical ACC transport estimates of Cunningham et al (2003) but less than more recent observations made by Donohue (2016) who suggest a Drake Passage transport closer to 170Sv.

Summary

The physical coupled model core of UKESM1, HadGEM3-GC3.1 at a resolution of N96 (~135km) in the atmosphere and 1° in the ocean (N96O1), has now been frozen. In this article we describe a number of key performance indicators from present-day (constant year 2000 forcing) runs of N96O1, indicating a very acceptable level of simulation accuracy. In the preceding article in this newsletter (Mulcahy et al.) we detailed some specific developments to the atmospheric component of N96O1 that were necessary to improve the pre-industrial to present-day radiative forcing signal. Both of these articles will be presented in more detail in the peer-reviewed literature in the coming

months. HadGEM3-GC3.1 is now ready for use as a coupled physical climate model, at both resolutions N216O025 and N96O1. Over the coming months the various Earth system components intended for UKESM1, namely modules for interactive stratosphere-troposphere chemistry, marine biogeochemistry, terrestrial carbon-nitrogen processes and dynamic vegetation and interactive continental ice sheets will be migrated from an earlier version of HadGEM3 and scientifically tuned with HadGEM3-GC3.1 (N96O1) in readiness for application within the CMIP6 project.

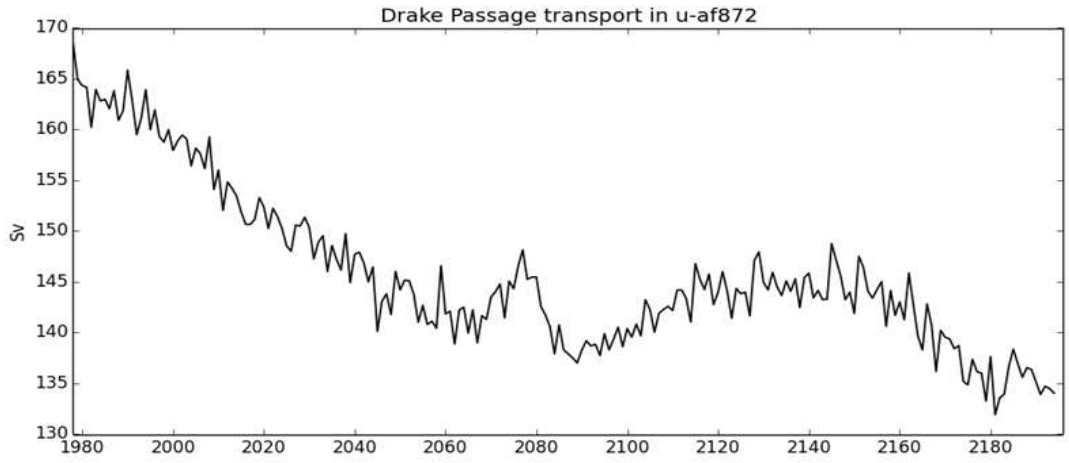

Figure 7. Zonal volume transport (Sv) through the Drake Passage associated with the ACC.

References:

Bryan, F.O. *et al*. (2007). Resolution convergence and sensitivity studies with North Atlantic circulation models: The western boundary current system. *Ocean Modelling*, 16(3-4):141 – 159

Buckley, M. W. and J. Marshall *(*2016). Observations, inferences, and mechanisms of the Atlantic Meridional Overturning Circulation: A review*. Rev. Geophys*.*,* 54

Cunningham, S. A*.,* S. G. Alderson*,* B. A. King*,* and M. A. Brandon *(*2003*).* Transport and variability of the Antarctic Circumpolar Current in Drake Passage*. J. Geophys. Res*.*,* 108*, 8084*

Donohue, K. A. *et al. (*2016). Mean Antarctic Circumpolar Current transport measured in Drake Passage. *Geophys. Res. Lett*., 43*,* 11,760–11,767*,*

Frajka-Williams, E. *et al*. (2016). Compensation between meridional flow components of the Atlantic MOC at 26° N. *Ocean Sci*., 12, 481-493,

Good, S. A., M. J. Martin and N. A. Rayner (2013). EN4: quality controlled ocean temperature and salinity profiles and monthly objective analyses with uncertainty estimates. *J. Geophys. Res: Oceans*, 118, 6704-6716

Marshall J.M and K. Speer (2012). Closure of the meridional overturning circulation through Southern Ocean upwelling. *Nature Geoscience*, 5, 171-180

Rayner, N. A. *et al.* (2003): Global analyses of sea surface temperature, sea ice, and night marine air temperature since the late nineteenth century. *J. Geophys. Res*. 108, No. D14, 4407